Analysis of Performance Enhancement of Clustered-Based Phased Arrays Employing Mixed Antenna Element Factor

Francesco Alessio Dicandia, *Member, IEEE*, and Simone Genovesi, *Senior Member, IEEE*

***Abstract*— A novel strategy for the design and optimization of large-scan phased arrays is proposed. Active electronically beam-scanning antennas offer an unparalleled set of degrees of freedom, but they can be expensive, require complex radiofrequency frontends, a suitable thermal management and generally undergo a loss in directivity due to the pattern shape of the unit radiating element. A solution to these problems can be offered by an approach that reduces the number of transmit/receive modules (TRMs) and phase shifters (PSs) by a simple and fast clustering strategy based on Penrose tessellation that operates on the regular lattice of the radiating elements. More importantly, the proposed scheme adopts a mixed-mode element factor that proves to be effective in guaranteeing a remarkable scan efficiency and robustness with respect to array elements failures. The optimization process aims to maximize the minimum gain along the main beam during the scan as well as minimizing the peak sidelobe level (PSLL), while reducing the number of TRMs.**

***Index Terms*—Penrose tiles, triangular lattice, phased array antenna, multiobjective optimization, wide angle scan.**

I. Introduction

Ever-increasing system performance requirements for wireless communications push the development of radiating platforms offering flexible, reliable, and cost-effective solutions [1]–[4]. Important features can be represented by adaptive properties offered by a single antenna able to reconfigure its operative frequency [5]–[7], radiation pattern [8]–[11], or polarization [12], [13]. Active electronically beam-scanning antennas are also a fundamental asset in the new communications paradigms [14]. Indeed, wide beam scanning range to provide a viable communication and fulfil the systems' needs, such as reliability and spectral efficiency represents an essential feature in most of the modern wireless systems and certainly will represent a key factor in driving their evolution with the advent of future 6G wireless technologies [15]. In a fully populated array (FPA) it is possible to independently control both feeding amplitude and phase of each radiating element by using a dedicated transmit/receive module (TRM), a solution that provides an excellent control of the radiated pattern at the price of a high cost. This architecture also requires for each individual antenna a phase shifter (PS) as well as a power amplifier (PA), thus furthering increasing the cost but also the overall loss determined by the high number of PSs and, possibly, a critical thermal and footprint management of the radiofrequency frontend [14]. Moreover, phased arrays undergo a decrease in directivity when large scan angles are approached due to the element factor, which is typically a cosine function [16]. These critical factors suggest seeking for other options than a FPA that can mitigate their downsides. An aperiodic arrangement of the array elements can help in coping with some of the aforementioned problems [17]–[20], although it can require complex feeding networks. The reconfigurability of the single element radiation pattern during the main beam scan can be introduced as an additional design resource [21], [22]. However, a pattern-reconfigurable element needs diodes or RF switches that cause a decrease of the overall system performance due to the insertion loss of the active element with respect to a static one.

The cost reduction and power saving goals can be achieved by the reduction of the TRMs number, since they count for almost half of the cost of a phased array [14]. To achieve this goal the array radiating elements lying on a regular and periodic lattice are grouped into different tiles or subarrays fed by a single TRM. A phased array can therefore be divided into identical and contiguous subarrays. However, although this approach eases the array manufacturing, reducing the cost and the power consumption with respect to an FPA, it can undergo limitations in angular scan range due to the onset of grating lobes inside the visible region [16] determined by the subarray periodicity. Overlapped subarrays have been investigated to overcome this drawback, [23], [24] but they need cumbersome feeding network, especially at millimeter wave frequencies [25], and may have limited scan. Irregular subarray partitions have been proposed [26]–[30] with the aim of maintaining acceptable the feeding network complexity, but at the same time preserving the wide-angle beam scanning capability. In fact, the aperiodicity introduced at the subarray level avoids the appearance of grating lobes and keeps at a reasonable level the

Francesco Alessio Dicandia is with Cnr-Istituto di Elettronica e di Ingegneria dell'Informazione e delle Telecomunicazioni, Pisa 56122, Italy (e-mail: francescoalessio.dicandia@cnr.it).

Simone Genovesi is with Dipartimento di Ingegneria dell'Informazione, University of Pisa, Pisa 56122, Italy (www.dii.unipi.it). (e-mail: simone.genovesi@unipi.it). Work partially supported by the Italian Ministry of Education and Research (MIUR) in the framework of the Crosslab and Forelab projects (Departments of Excellence).

radiation pattern lateral lobes. However, it has to be noticed that sometimes the computational cost of individuating the most suitable partitioning scheme can be considerable since the irregular partition of a phased array is an open-ended problem [31], [32]. Recently, a clustering technique exploiting the Penrose tessellation for the partitioning of a periodic phased array into irregular subarrays has been proposed [33] as a solution for overcoming or mitigating the FPA critical issues. The Penrose element arrangement can easily provide irregular partitions of arrays with elements on a regular lattice by exploiting a tessellation obtained with a deterministic procedure. The number of TRM and PS is clearly reduced because of the partition policy that consider a single PS for each subarray.

The proposed work aims to address the directivity scan loss in the framework of multiobjective optimization problem aimed to maximize the minimum gain along the main beam direction during the scan as well as minimizing the peak sidelobe level (PSLL) and the number of TRMs but, at the same time, avoiding the use of RF switches. The envisioned approach is based on the use of two different radiating elements that exhibit a static radiation pattern. It is worth mentioning that this is the first time that a static mixed-antenna element pattern has been exploited in the design of phased arrays.

The paper is organized as follows. Section II describes the procedure that provides the irregular array partitioning by using the Penrose tessellation and introduces the exploitation of two different antenna elements with static radiation patterns. The assessment of the achievable performance and the benefit offered by the proposed array configuration are reported in Section III for two different scenarios, namely the former requiring an angular scan up to 60° and the latter going up to 75°. Section IV offers a statistical analysis of the mixed-element configurations and the average performance of an array employing a mixed-element pattern with respect to a single one. The robustness of the proposed design approach is also tested by considering the failure of up to four TRMs (*i.e.*, four subarrays) and final conclusions are drawn in Section V.

II. Irregular Partitioning with Mixed Antenna Element Factors Design Strategy

The radiation pattern (RP) radiated by a subarrays-based phased array comprising Q tiles number lying on xy plane is equal to:

$$RP(u,v)=\sum_{q=1}^{Q} I_q e^{j\alpha_q} \sum_{n=1}^{N_q} E_{q,n}(u,v)\, e^{j\beta\left(x_{q,n}u+y_{q,n}v\right)} \quad (1)$$

where $u=\sin(\theta)\cos(\phi)$, $v=\sin(\theta)\sin(\phi)$, $\beta=2\pi/\lambda_0$ is the wave number, I_q, α_q and N_q represent the amplitude, the phase and the number of radiating elements of the q^{th} tile, respectively, $E_{q,n}(u,v)$ the n^{th} element radiation pattern within the q^{th} tile, whereas $x_{q,n}$ and $y_{q,n}$ are the related antenna element geometrical coordinates that depend on the employed array lattice. The radiation element phase (α_q) related to the q^{th} subarray, and hence to all the radiating elements (N_q) belonging to the selected subarray, depends on its centroid ($x_{q,0}$, $y_{q,0}$) to steer the main beam in the desired direction (θ_0,ϕ_0) as follows:

$$\alpha_q=\beta\left[x_{q,0}\sin(\theta_0)\cos(\phi_0)+y_{q,0}\sin(\theta_0)\sin(\phi_0)\right] \quad (2)$$

In the proposed design strategy, the benefit of adopting an aperiodic tessellation capable to cover a plane with a deterministic policy [34] has been exploited to provide irregular partitions of a phased array. Indeed, in general, the subarrays-based phased arrays allow considerably reducing both the cost and the array architecture complexity by providing a more balanced cost and performance trade-off. Specifically, the version known as "thick and thin" composed by a pair of isosceles triangles, namely with internal angles 36°, 36°, 108° and 72°, 72, and 36° that are able to cover a plane without overlaps or gaps, has been exploited for the phased array partitioning optimization.

In addition to the clustering technique based on a Penrose tessellation, in order to extend the scanning range, the selection of one between two alternative radiation patterns for all the phased array radiating elements is exploited. Specifically, two possible radiation patterns for each radiation element can be selected, namely a patch-like (EF_1) or a monopole-like (EF_2) one, as follow:

$$\begin{aligned} EF_1(\theta)&=\cos(\theta)^{0.5} \\ EF_2(\theta)&=\sin\left(\frac{3}{2}\theta\right)^{3.5} \end{aligned} \quad (3)$$

where the exponent 3.5 for EF_2 has been selected to guarantees the same antenna element factor maximum gain of 6 dBi. The employed mixed antenna element factors as a function of the θ angle are shown in Fig. 1.

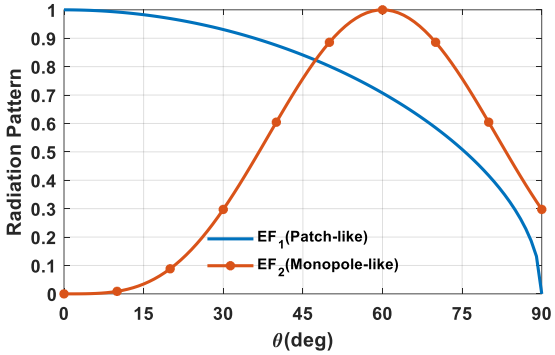

Fig. 1. Example of the two considered element radiation patterns as a function of θ angle.

As it can be seen, the patch-like mode presents a maximum radiation toward $\theta=0°$ whereas the monopole-like element factor is characterized by a maximum radiation at $\theta=60°$. Some examples of antenna design with radiated fields shape quite similar to the adopted ones, namely a patch-like (EF_1) or a monopole-like (EF_2) mode, are reported in [35]–[37]. It is worth mentioning that the novelty addressed in this paper is not mainly related to the two alternative radiation patterns shapes shown in Fig. 1 (EF_1 and EF_2). In fact, they are used just as example to emphasize the potential radiative performance of the proposed phased array architecture based on a mixed element factor. Therefore, in general, according to the operative scenarios and the required system needs, different mixed

antenna element factors could be employed.

The novel clustered-based phased array architecture employing mixed antenna element factors is generated through a recursive algorithm as follows:

1) define the isosceles triangular side length L and overlap the Penrose tessellation vertexes with the regular and periodic phased array lattice;
2) create a list with the antenna elements that can be used for the phased array partition. At the beginning, the list contains all the antenna elements of the array;
3) generate two binary variables x_n and $y_m \in \{0,1\}$, where x_n ($n = 1,\ldots,K$) being K the total number of vertexes of the tessellation, and y_m ($m = 1,\ldots,N$) being N the total number of antenna elements. y_m defines the antenna elements radiation pattern of the array, *i.e.*, $y_m = 1$ for EF_1 whereas $y_m = 0$ for EF_2.
4) call a recursive partition function for all the selected vertex $x_n = 1$ by starting from the first one in the list:
    a. identify all the isosceles triangles of the tessellation that have in common the picked vertex,
    b. all the antenna elements of the periodic array inside the selected isosceles triangles form a subarray,
    c. remove the selected antenna elements of the periodic array from the list of the available antenna elements for the phased array partition.
5) if the list of the available antenna elements for the phased array partition is not empty, assign a single element subarray for all the elements.

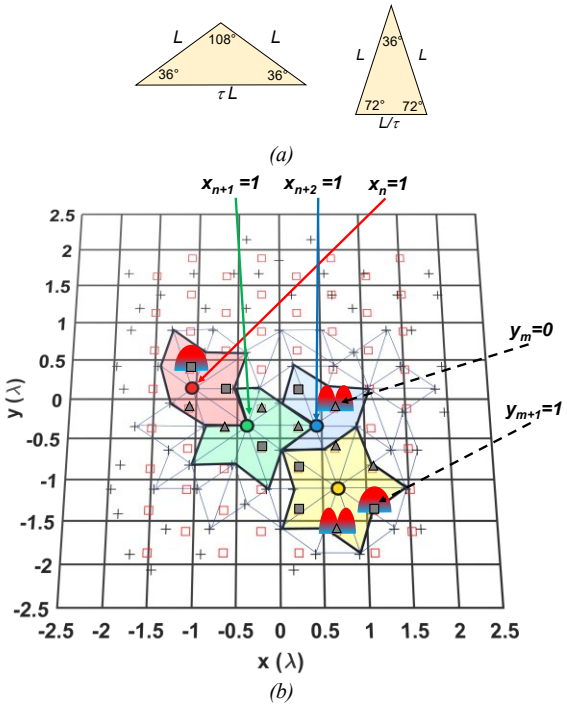

Fig. 2. Penrose tessellation of the array: *(a)* triangles of the "thick and thin" version of Penrose, where the variable τ represents the ratio of the area of both triangles and *(b)* example of a possible tessellation where red squares refer to the triangular periodic element lattice whereas the black crosses ones to the Penrose's triangle vertexes. The grey squares are the patch-like elements, whereas the triangles are the monopole like ones.

For better clarify the algorithm used for the synthesis of the proposed clustered-based phased array architecture, an example of partition of an array composed by 8×8 elements arranged in a triangular lattice is shown in Fig. 2. In particular, the two triangles of the "thick and thin" Penrose tessellation are reported in Fig. 2*a* whereas the red squares and the black cross ones refer to the regular and periodic triangular lattice array and the vertexes of a Penrose's tiles, respectively (Fig. 2*b*). Moreover, both the interelement spacing among antenna element and the Penrose's isosceles triangles sides length L is equal to 0.5 λ_0. In the first three iterations of the algorithm of Fig. 2 the highlighted areas (*i.e.*, red, green and blue) host the antenna elements that form the three different subarrays. They are realized from the picked Penrose's triangle vertex through the binary variable x_n, x_{n+1} and x_{n+2}. Meanwhile, the binary variable y_m defines the antenna elements radiation pattern of whole array (*i.e.,* grey triangles for the monopole-like, grey square for patch-like). It is worthwhile to mention that in the clustered-based phased array multiobjective optimizations, the selection of one of the two alternative radiation patterns, through the binary variable y_m, is not subject to any constraint or selection policy. Therefore, each phased array partition layout, as well as in every single tile, could host elements factor with the numerosity and ratio guided by the Pareto front algorithm. However, in case of some radiative constraints, such as the minimum array gain value at broadside direction ($\theta = 0°$), some selection policies could be introduced in the Pareto optimization problem.

In the following sections it will be highlighted as the Penrose's triangle sides length L and the mixed antenna element factor affect the radiation performance while reducing the number of TRMs. It is worth noting that, in the following, since the mutual coupling among radiating elements is more related to a particular antenna array design perspective instead of the addressed theoretical study, the arrays performance are evaluated under the assumption of identical element factors (*i.e.*, EF_1 and EF_2) for all the corresponding radiating elements.

III. 16×16 Subarray-Based Phased Array with Mixed Antenna Element Factor

The novel strategy for improving the performance of a large-scanning phased array has been applied to the case of a 16×16 array of radiating elements arranged in a triangular lattice with an interelement spacing of 0.5 λ_0. The 16×16 phased array optimization has been carried out by exploiting the multi-objective algorithm based on the Pareto dominance concept [38] implemented in MATLAB. Specifically, the parameters defined in a-priori set are: *(i)* the total number of phased array elements (N), *(ii)* phased array lattice (*i.e.*, triangular) and element spacing (0.5 λ_0), *(iii)* side of the Penrose tessellation (L) and *(iv)* the angular scan region. The parameters to be optimized (*i.e.*, the search space) are: *(i)* the vector $\underline{X}$ that determines the tessellation and *(ii)* the vector $\underline{Y}$ that determines the kind of array element. The conflicting objectives of the Pareto optimal solutions are: *(i)* maximizing the minimum array gain along the main beam direction evaluated inside the

predefined scenario where the phased array can steer, *(ii)* the number of subarrays (*i.e.,* feeding points or TRMs) as well as *(iii)* the peak side lobe levels (PSLL) in the visible region. A flowchart describing the Penrose clustered phased array optimization based on the Pareto dominance concept is depicted in Fig. 3.

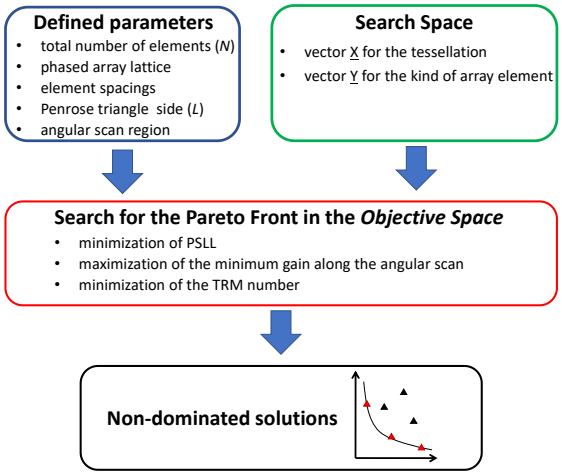

Fig. 3. Flowchart describing the Penrose clustered phased array optimization based on the Pareto front algorithm.

In the following, two operative scenarios comprising a predefined circular scanning area in the *uv* plane with a maximum steering angle of 60° and 75° have been considered to assess the novel phased array architecture.

A. Case 1: Maximum Steering Angle of $\theta_0 = 60°$

In this subsection, a circular scenario with a maximum steering angle of $\theta_0 = 60°$ is considered. By using the algorithm described in Section II, the two Pareto fronts that highlight the trade-off among the three conflicting objectives, namely minimum array gain, number of subarrays and the PSLL as a function of the number of subarrays, are reported in Fig. 4 for different values of the triangle side length *L*. To implement the partition of the array, a uniform amplitude excitation at the subarrays' level has been considered [33]. More in detail, Fig. 4 compares two Pareto fronts by considering the mixed-mode antenna reported in Fig. 1 (*i.e.*, patch-like and monopole-like patterns) and a single-mode antenna element factor by employing only EF_1 (*i.e.*, patch-like only). As expected, the phased array undergoes a decreasing of the minimum gain achievable along the main beam during the scan inside the visible region for both approaches by reducing the number of subarrays. However, the dual-mode antenna element factor allows enhancing the minimum value of the achievable array gain, hence reducing the scan loss. Specifically, for large number of subarrays (higher than 170 TRMs) the two Pareto fronts differ in gain about 0.6 dB. However, reducing the number of irregular and contiguous subarrays causes a higher and higher gain difference in favor of the phased array with mixed-antenna element factors. The largest difference between the minimum gain offered by the two strategies is more than 2 dB in case of 100 subarrays in favor of the mixed-element one. It is important to highlight that this solution reduces of around 60 % the feed points with respect to the FPA. In addition to a lower scan loss, Fig. 4*b* emphasizes that the mixed antenna element factor architecture turns out to be advantageous also from the PSLL point of view. Indeed, for almost all the array partitioning, the achieved PSLL during the steering inside the circular scenario in case of a mixed antenna element factor is lower than the single mode.

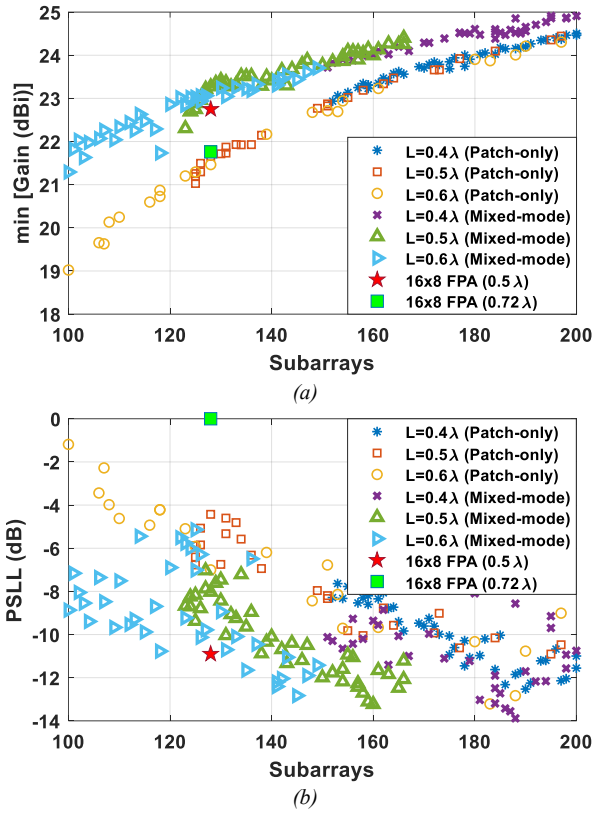

Fig. 4. Pareto fronts obtained by considering a 16×16 clustered phased arrays for different Penrose isosceles triangle sides length *L* in case of a single-mode antenna elements factor EF_1 (Patch-only) and a mixed-mode antenna radiation pattern elements (EF_1 and EF_2) with a maximum scan beam up to $\theta_0 = 60°$; *(a)* minimum array gain along the main beam during the scan versus number of subarrays and *(b)* PSLL versus number of subarrays.

Moreover, the reduction of the subarrays causes a severe PSLL worsening for a single mode array solution. On the contrary, the PSLL degradation in case of the proposed mixed antenna element mode, is considerably lower. Specifically, the mixed mode can ensure a PSLL <– 10 dB by employing at least 118 feed points, whereas by employing only a patch antenna element factor, the condition of PSLL <– 10 dB is guaranteed by using at least 158 subarrays, namely around 34 % more of feed points. For comparison, Fig. 4 also shows the radiative performance of a FPA with 16×8 elements (*i.e.*, 128 TRMs) comprising patch-like radiation patterns (*i.e.*, EF_1 only) in case of an interelement spacing of 0.5 λ_0 and 0.72 λ_0. Specifically, although both the FPAs with half TRMs (*i.e.*, 128) provides a superior minimum array gain along the main beam direction than the clustered-based 16×16 phased array with a single-element antenna pattern (*i.e.*, EF_1 only), especially for the one with an interelement spacing of 0.5 λ_0, the novel clustered-based phased array configuration employing mixed antenna element factors allows enhancing the overall minimum array gain value. Concerning the PSLL (Fig. 4*b*), the 16×8 FPA with 0.5 λ_0 elements spacing ensures a

PSLL <– 10.9 dB instead of a PSLL <– 9.8 dB in case of a mixed antenna element mode. Nevertheless, the halves of the array aperture in case of 16×8 FPA determines a larger radiations footprint, namely a worse angular scan resolution of the main beam than clustered-based 16×16 phased arrays. Moreover, this also leads to an almost double power consumption density [39], thus requiring more complicated heat dissipation mechanisms. On the contrary, the 16×8 FPA with the same area of the clustered-based 16×16 phased arrays, achieved with an interelement spacing of 0.72 λ_0, suffers of grating lobes onset due to a PSLL = 0 dB.

The radiation performance of a clustered-based phased arrays composed by 118 feed points is examined in the following. The normalized gain value as a function of the main beam direction with a maximum scan beam up to $\theta_0 = 60°$ is illustrated in Fig. 5 for both the phased array architectures. In general, the arrays' gain present higher values along the broadside direction ($\theta_0 = 0°$), and then, it fades little by little during the main beam steering due to the beam widening and to the lower element's gain [40]. More in detail, the scan loss in case of a mixed antenna element factors (Fig. 5*a*) is slightly more than 3 dB whereas, the patch-only antenna mode is characterized by a scan loss more than 7 dB in case of scanning angles close to 60°.

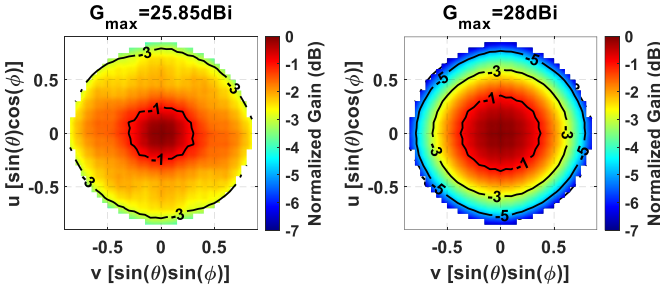

Fig. 5. Normalized array gain as a function of the steering angle with a maximum scan beam up to $\theta_0 = 60°$ by exploiting the Penrose clustering-based 16×16 triangular lattice array with 118 subarrays; *(a)* mixed-mode antenna elements factor and *(b)* patch-only antenna element factor.

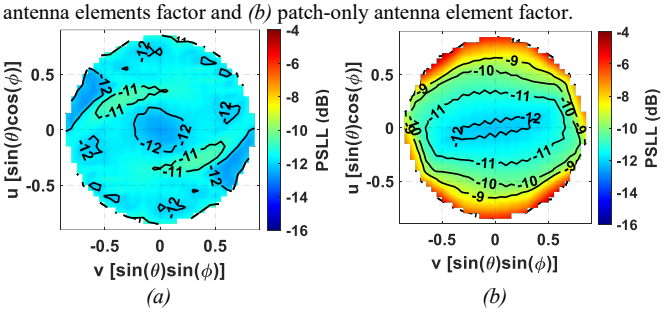

Fig. 6. PSLL as a function of the steering angle with a maximum scan beam up to $\theta_0 = 60°$ by exploiting the Penrose clustering-based 16×16 triangular lattice array with 118 subarrays; *(a)* mixed-mode antenna elements factor and *(b)* patch-only antenna element factor.

The lower scan loss as a function of beam steering provided by a mixed-mode phased array could be beneficial also in terms of transceiver linearity and power consumption, both pivotal features for the next wireless communication systems [41], [42]. In fact, due to the array gain decrease during the scan, the output power required to preserve the same equivalent isotropic radiated power (EIRP) turns out to be dependent on the main beam direction. This may lead to a large dynamic of the PAs output power and hence to a dissimilar signal distortion and PAs efficiency [43] in the scanning area, under the assumption of a fixed PAs operation point. Therefore, the reduced output power dynamic offered by the mixed-mode element architecture favours the transceiver linearity improvement as well as a less power hungry. Even though the mixed-mode architecture provides a small scan loss, the maximum gain value of the array achieved at broadside ($\theta_0 = 0°$) is 25.85 dBi whereas the patch-only antenna element pattern provides about 2 dB more maximum gain. The lower maximum gain value is inevitable since the array antenna elements with monopole-like (EF_2) radiation pattern does not radiate toward broadside. However, the adoption of some element factor selection criteria during the optimization or the employment of two other elements with a more overlapping radiation pattern, could compensate the gain reduction at broadside.

The PSLL as a function of the steering angle by exploiting the Penrose clustering-based 16×16 triangular lattice array with 118 subarrays is depicted in the color maps of Fig. 6. As it is evident, despite a feeding points reduction of more than 50 %, Penrose clustered arrays with a mixed antenna element factor (Fig. 6*a*) allows a remarkable PSLL < – 10dB. Conversely, the patch-only antenna case (Fig. 6*b*) undergoes a PSLL worsening, suffering a PSLL of – 4 dB.

The normalized radiation patterns (RPs) of two partitions arrangement of a Penrose clustering-based 16×16 triangular lattice array with 118 and 139 subarrays evaluated for broadside ($\theta_0 = 0°$) and $\theta_0 = 60°$ scan angle at $\phi = 0°$ plane are shown in Fig. 7.

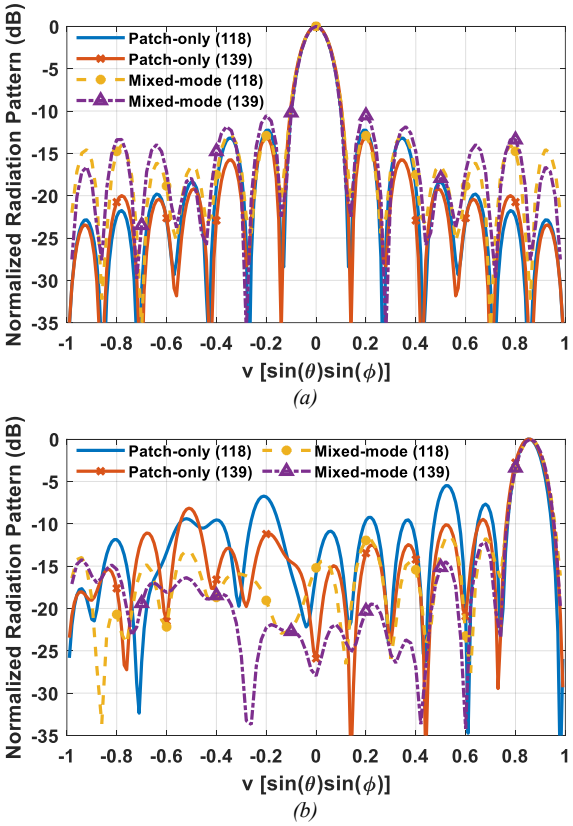

Fig. 7. Normalized RP with a Penrose clustering-based 16×16 triangular lattice array with 118 and 139 subarrays in case of a single-mode antenna elements factor EF_1 (Patch-only) and a mixed-mode antenna radiation pattern elements

(EF_1 and EF_2); *(a)* $\theta_0 = 0°$ scan angle and *(b)* $\theta_0 = 60°, \phi = 0°$ scan angle.

Additionally, the normalized RPs when the main beam is steered at the edges of the field of view are reported in the color maps of Fig. 8. It is apparent that, despite the large scanning, the lateral lobes turn out to be well below the main beam especially for a mixed-mode antenna elements factor (Fig. 8*a*,*b*,*i*,*l*). Conversely, the patch-only case (Fig. 8*c*,*d*,*m*,*n*) determines a greater radiation spreading over the visible region with the presence of different high lateral lobes especially for the case of 118 feed points (Fig. 8*c*,*d*) to the point that the main beam direction cannot be uniquely identified. The performance improvement exhibited by the mixed antenna element factor is also appealing in a multiusers scenario where a lowering of the average interference over the visible region is beneficial for an improved quality of service [44]. Fig. 8 also shows the array clustering layout and the corresponding antenna element factors for both the array partitions.

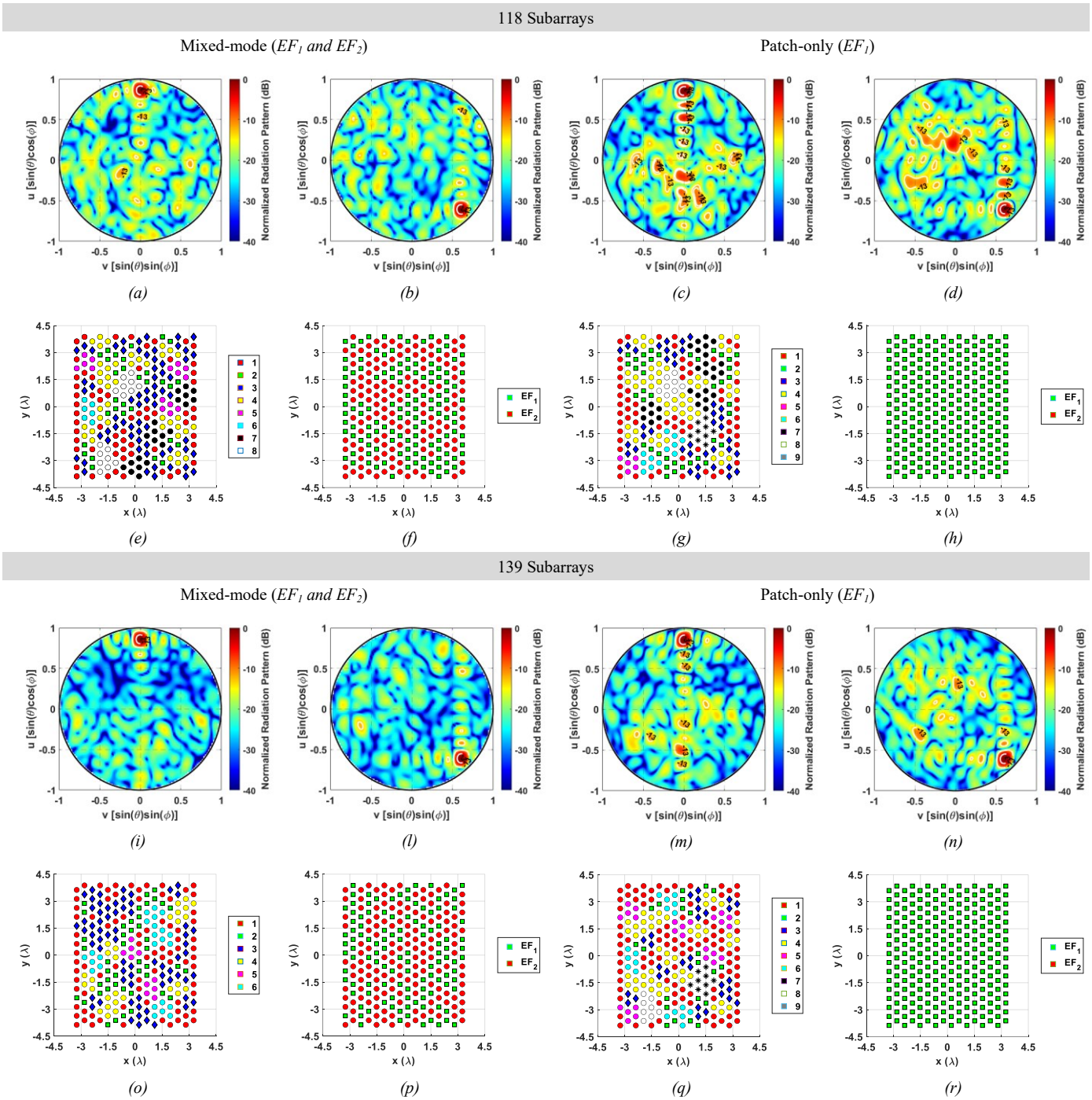

Fig. 8. Normalized radiation pattern evaluated at $\theta_0 = 60°, \phi_0 = 0°$ and $\theta_0 = 60°, \phi_0 = 135°$ by exploiting the Penrose tiling subarrays in case of 16×16 elements by considering *(a)*,*(b)*,*(i)*,*(l)* a mixed-mode antenna elements factor and *(c)*,*(d)*,*(m)*,*(n)* a patch-only antenna element factor for 118 and 139 subarrays number; *(e)*,*(g)*,*(o)*,*(q)* array clustering layout whereas *(f)*,*(h)*,*(p)*,*(r)* antenna element factors.

To better appreciate the improvement of the mixed-mode approach, Table I summarizes the radiation performance in terms of TRMs number, maximum and minimum array gain, scan loss and PSLL for both the mixed-mode and single-mode antenna element factor architecture. In addition, the FPA array radiative performance in case each radiation element has a patch-like (EF_1) radiation pattern are reported for comparison.

TABLE I
PERFORMANCE COMPARISON FOR DIFFERENT TRMS IN CASE OF A MIXED-MODE (EF_1 AND EF_2) AND A SINGLE-MODE ANTENNA ELEMENT FACTOR (EF_1 ONLY) 16×16 PHASED ARRAY WITH A MAXIMUM STEERING ANGLE OF $\theta = 60°$.

TRMs	Phased Array Architecture	Max Gain (dBi)	Min Gain (dBi)	Scan Loss (dB)	PSLL (dB)
100	Single-Mode	28	19	9	-1.7
	Mixed-Mode	25.38	21.4	3.98	-8.5
137	Single-Mode	28.23	22.05	6.18	-7.36
	Mixed-Mode	25.58	23.36	2.22	-10.45
160	Single-Mode	28.2	23.33	4.87	-8.8
	Mixed-Mode	26.48	24	2.48	-13.22
200	Single-Mode	28.2	24.4	3.8	-11
	Mixed-Mode	26.9	24.9	2	-10.8
256	FPA	28.48	25.4	3.08	-11.2

B. *Case 2: Maximum Steering Angle of $\theta_0 = 75°$*

With the aim of further assessing the performance improvement of clustered-based phased arrays by employing mixed antenna element factor a circular scenario with a maximum steering angle of $\theta_0 = 75°$ is considered in this sub-section.

Fig. 9 displays the two Pareto fronts highlighting the trade-off among the minimum array gain, number of subarrays and the PSLL as a function of the number of subarrays in case of a 16×16 clustered phased arrays. As in the pareto fronts of Fig. 4, the dual-mode antenna element factor architecture (*i.e.*, EF_1 and EF_2) outperforms the single-mode one by employing only EF_1. Additionally, a more pronounced difference of the minimum gain in favour of the mixed-mode strategy is visible in Fig. 9*a*. In fact, in case of a clustered phased array characterized by 180 subarrays the two Pareto fronts provide a gain difference of 2.1 dB. However, by reducing more and more the subarrays number there is an almost linear increasing of the gain difference up to reach a value of around 5 dB in favor of a mixed-mode array partition in case of 100 subarrays. The mixed-mode element factor proves to be effective also in keeping at acceptable levels the PSLL during the steering inside the circular scenario, as illustrated in the Pareto fronts of Fig. 9*b*. Indeed, as for the case of $\theta_0 = 60°$ (Fig. 4*b*), the reduction of the subarrays causes a serious PSLL worsening for a single mode array solution without ever reaching a PSLL <– 10 dB and suffering from grating lobes for 100 subarrays. On the contrary, the mixed antenna element scheme is capable to guarantee a PSLL <– 10 dB during the beam steering inside the circular scenario by employing an array partition with at least 162 subarrays. In addition, array partitions with lower subarrays provides a mild deterioration of the PSLL up to around −5.5 dB with 100 TRMs.

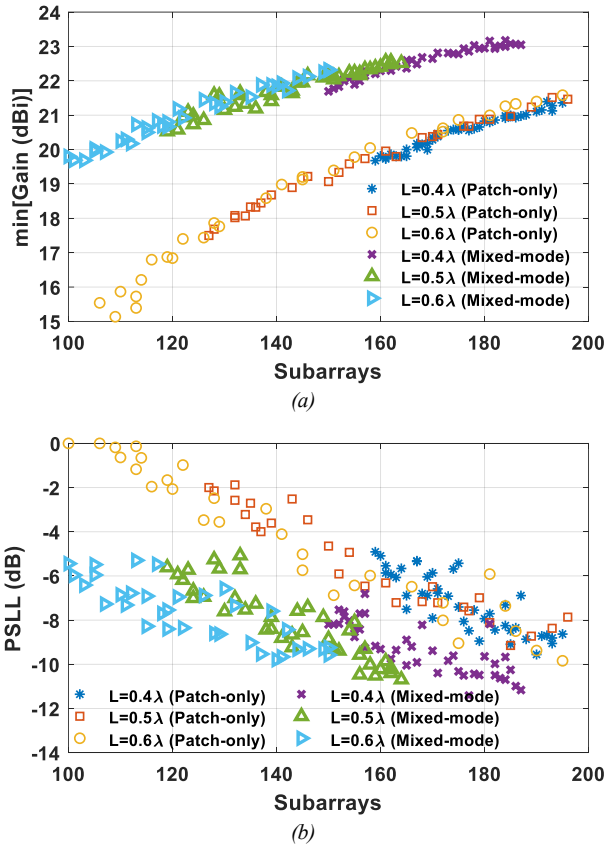

Fig. 9. Pareto front by considering a 16×16 clustered phased arrays for different Penrose isosceles triangle sides length L in case of a single-mode antenna elements factor EF_1 (Patch-only) and a mixed-mode antenna radiation pattern elements (EF_1 and EF_2) with a maximum scan beam up to $\theta_0 = 75°$; *(a)* minimum array gain versus number of subarrays and *(b)* PSLL versus number of subarrays.

It is worth noting that if some applicative scenarios need to a lower PSLL within the whole the scanning area some amplitude tapering techniques could be used to further reduce the lateral lobes [30], [33], [45], [46]. However, as remarked in [33], the amplitude effect on PSLL lowering gradually vanishes with the reduction of the employed TRMs.

The normalized RP of a clustered-based phased arrays composed by 118 subarrays when the main beam is steered at ($\theta_0 = 75$, $\phi_0 = 45°$) is examined in Fig. 10*a* for both the phased array architectures. As it can be inferred from the color maps, the patch-only antenna element factor (Fig. 10*a* right column) provides a considerable radiation spreading in the visible region to the point that the desired main beam direction cannot be clearly identified. Conversely, the mixed-mode antenna elements factor (Fig. 10*a* left column) focusses better the energy toward the desired main beam direction by generating just three undesired lateral lobes with a PSLL of around –9 dB. The corresponding arrays partition layout and the antenna element factors are depicted in Fig. 10*b*-*c*.

Table II reports the radiation performance comparison for a 16×16 Penrose clustered phased array in terms of maximum and minimum array gain, scan loss and PSLL between the mixed-mode and the single-mode antenna element factor for

some TRMs number. In addition, the FPA array radiative performance in case each element has a patch-like (EF_1) radiation pattern are reported for comparison.

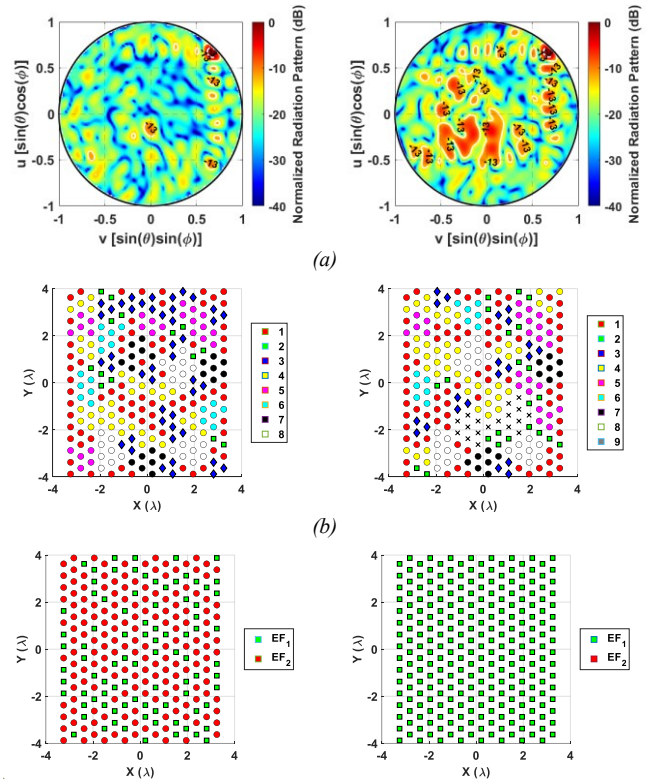

Fig. 10. Normalized radiation pattern for a 16×16 Penrose clustered phased arrays with 118 subarrays in case of a patch-only antenna elements factor (right column) and a mixed-mode antenna elements factor (left column) for scan angle of *(a)* $\theta_0 = 75°$ at $\phi = 45°$ plane, *(b)* the array clustering layout and *(c)* the antenna element factors.

TABLE II

PERFORMANCE COMPARISON FOR DIFFERENT TRMS IN CASE OF A MIXED-MODE (EF_1 AND EF_2) AND A SINGLE-MODE ANTENNA ELEMENT FACTOR (EF_1 ONLY) 16×16 PHASED ARRAY WITH A MAXIMUM STEERING ANGLE OF $\theta = 75°$.

TRMs	Phased Array Architecture	Max Gain (dBi)	Min Gain (dBi)	Scan Loss (dB)	PSLL (dB)
120	Single-Mode	28.02	16.98	11.04	-2.54
	Mixed-Mode	23.73	21.37	2.36	-8.04
160	Single-Mode	28.33	20	8.33	-6.22
	Mixed-Mode	25.27	22.72	2.55	-11.4
180	Single-Mode	28.35	20.94	7.41	-8.07
	Mixed-Mode	25.31	23.28	2.03	-11.32
256	FPA	28.48	23.1	5.38	-9.8

IV. STATISTICAL ANALYSIS AND FAILURE ASSESSMENT

The selection of the antenna element between the two available options was not subject to any constraint in the optimization process. Each subarray could host any of them and in the numerosity suggested by the Pareto front algorithm. It is therefore interesting to observe that (Fig. 11*a*) among all the array configurations, and for all the adopted tessellations, the monopole-like array element (*i.e.*, EF_2) has been selected more times than the patch-like ones. Moreover, this trend is much more visible by incrementing L (Fig. 11*b*), since the probability of having a majority of patch elements decreases with the increase of the side length of the tessellation.

A statistical analysis has been carried out to additionally highlight the advantages of the proposed subarray strategy. Specifically, the circular scanning area in which the phased array can steer the main beam has been discretized with a sampling step of 5° for both θ and ϕ, respectively, to collect the radiative performance. By referring to the case of all the array partition layouts with a length $L = 0.6\ \lambda$, it is possible to observe from the cumulative distribution function (CdF) that in the 80% of the scans within the circular scenario with a maximum steering angle of $\theta_0 = 60°$ (CdF = 0.8) the mixed-mode approach guarantees a PSLL between −13 dB and −7 dB (Fig. 12*a*) whereas the single-mode one goes from −15 dB up to −3 dB (Fig. 12*b*). This means that during the scan on the whole visible region, the mixed-mode offers a much better worst-case scenario.

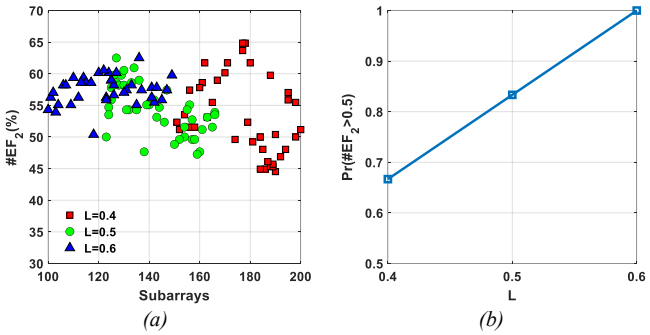

Fig. 11. *(a)* Percentage probability of having monopole elements (EF_2) in the array partition layouts and *(b)* array partition probability having a majority of EF_2 as a function of Penrose isosceles triangle sides length L. The analysis refers to the Penrose clustering-based 16×16 triangular lattice array with maximum steering angle of $\theta_0 = 60°$.

If the case of the array with 118 TRMs is considered as a representative one, being the one that exhibits a PSLL lower than −10 dB with the lowest number of subarrays, it can be seen that the PSLL of the mixed-mode array always outperforms the patch-like one during the scan (Fig. 13*a*) and that in around the 30% of the pointing directions it is also better in terms of gain (Fig. 13*b*) as well as providing a superior minimum gain value.

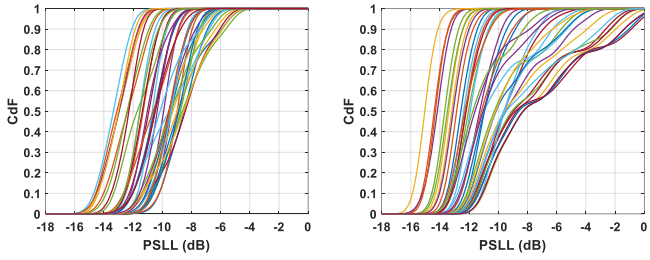

Fig. 12. CdF of the PSLL evaluated within the circular scenario with a maximum steering angle of $\theta_0 = 60°$ as a function of the array partition layouts by considering a 16×16 clustered phased arrays with a Penrose isosceles triangle sides length $L = 0.6\ \lambda$ in case of *(a)* mixed-mode antenna radiation pattern elements (EF_1 and EF_2) and *(b)* a single-mode antenna element factor EF_1 (patch-only).

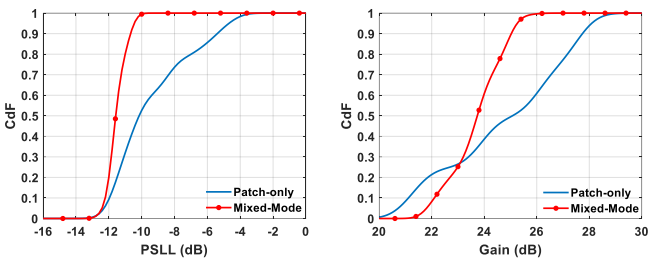

Fig. 13. CdF of the *(a)* PSLL and the *(b)* gain for a 16×16 Penrose clustered phased arrays with 118 subarrays in case of a patch-only antenna elements factor and a mixed-mode antenna elements factor for a circular scenario with a maximum steering angle of $\theta_0 = 60°$.

Finally, an assessment of the performance of the addressed array partitioning scheme has been done looking at the robustness with respect to failures of some TRMs [47]. More in detail, the first ten larger subarrays have been selected, regardless of the kind of hosted antenna elements. Then, for each pointing direction of the main beam, all the possible combinations of them including two, three and four subarrays among the selected ones have been considered and switched off. This means that in the case of the failure of four subarrays, up to thirty elements (around 12% of the total) are not contributing to the shaping radiation pattern. It is apparent from Fig. 14 that the presented paradigm provides a phased array that, despite a feeding points reduction of more than 50 % with respect to the FPA, is also able to endure the failure of several elements by keeping the PSLL lower than −10 dB, with very few exceptions, and never higher than −9.5 dB.

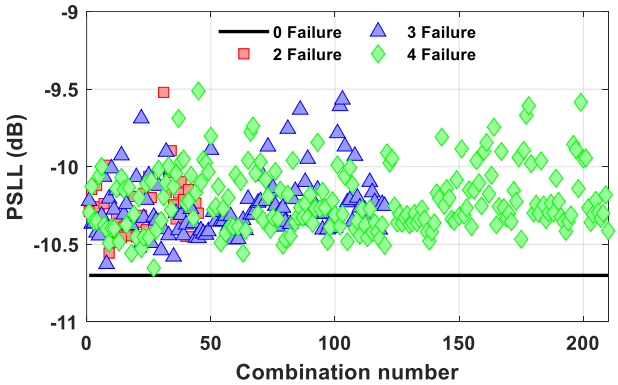

Fig. 14. PSLL within the circular scenario with a maximum steering angle of $\theta_0 = 60°$ in case of two, three and four damaged subarrays for a 16×16 Penrose clustered phased arrays with 118 subarrays and a mixed-mode antenna elements factor.

V. Conclusion

A solution to some of the problem that affects large-scan phased arrays has been proposed. The described strategy offers the possibility to lower the phased array cost by reducing the number of transmit/receive modules (TRMs) and phase shifters (PSs) by resorting to a subarray partitioning exploiting the Penrose tessellation. This task does not require a significant computational effort and operates on regular array lattices. More importantly, the envisioned scheme adopts a mixed-mode element factor that exploits the use of two different array elements with a non-reconfigurable pattern. This means that no additional RF switches must be implemented thus further contributing to an energy-efficient radiating platform, together with the reduction of PS because of a reduction in TRMs.

The performance assessment has shown a significant advantage with respect to designs based on a single-element antenna pattern in terms of TRMs reduction, minimum PSLL and maximum of the minimum gain during the wide-angle scan of the main beam. Specifically, by employing less than 50% of the TRMs of a FPA, a better minimum gain along the main beam (more than 5 dB) and lower PSLL (more than −5 dB) is provided by the proposed clustered-based phased arrays employing mixed antenna element factor.

The mixed-mode phased array scheme has also proven to be robust with respect to subarray failures, exhibiting a decreasing of the PSLL less than 1 dB even when 12% of elements switched off.

References

[1] F. A. Dicandia and S. Genovesi, 'Exploitation of triangular lattice arrays for improved spectral efficiency in massive MIMO 5G systems', *IEEE Access*, vol. 9, pp. 17530–17543, 2021.

[2] W. Hong *et al.*, 'Multibeam Antenna Technologies for 5G Wireless Communications', *IEEE Trans. Antennas Propag.*, vol. 65, no. 12, pp. 6231–6249, Dec. 2017.

[3] F. A. Dicandia, N. J. G. Fonseca, M. Bacco, S. Mugnaini, and S. Genovesi, 'Space-Air-Ground Integrated 6G Wireless Communication Networks: A Review of Antenna Technologies and Application Scenarios', *Sensors*, vol. 22, no. 9, Art. no. 9, Jan. 2022.

[4] Y. J. Guo, M. Ansari, R. W. Ziolkowski, and N. J. G. Fonseca, 'Quasi-optical multi-beam antenna technologies for B5G and 6G mmwave and THz networks: a review', *IEEE Open J. Antennas Propag.*, vol. 2, pp. 807–830, 2021.

[5] Q. H. Dang, S. J. Chen, D. C. Ranasinghe, and C. Fumeaux, 'A frequency-reconfigurable wearable textile antenna with one-octave tuning range', *IEEE Trans. Antennas Propag.*, vol. 69, no. 12, pp. 8080–8089, Dec. 2021.

[6] T. K. Nguyen, C. D. Bui, A. Narbudowicz, and N. Nguyen-Trong, 'Frequency-reconfigurable antenna with wide- and narrowband modes for sub-6 GHz cognitive radio', *IEEE Antennas Wirel. Propag. Lett.*, vol. 22, no. 1, pp. 64–68, Jan. 2023.

[7] S. Genovesi, A. Monorchio, M. B. Borgese, S. Pisu, and F. M. Valeri, 'Frequency-reconfigurable microstrip antenna with biasing network driven by a PIC microcontroller', *IEEE Antennas Wirel. Propag. Lett.*, vol. 11, pp. 156–159, 2012.

[8] L. Santamaria, F. Ferrero, R. Staraj, and L. Lizzi, 'Electronically pattern reconfigurable antenna for IoT applications', *IEEE Open J. Antennas Propag.*, vol. 2, pp. 546–554, 2021.

[9] Z. Ding, R. Jin, J. Geng, W. Zhu, and X. Liang, 'Varactor loaded pattern reconfigurable patch antenna with shorting pins', *IEEE Trans. Antennas Propag.*, vol. 67, no. 10, pp. 6267–6277, Oct. 2019.

[10] F. A. Dicandia, S. Genovesi, and A. Monorchio, 'Advantageous exploitation of characteristic modes analysis for the design of 3-D null-scanning antennas', *IEEE Trans. Antennas Propag.*, vol. 65, no. 8, pp. 3924–3934, Aug. 2017.

[11] F. A. Dicandia and S. Genovesi, 'A compact cubesat antenna with beamsteering capability and polarization agility: characteristic modes theory for breakthrough antenna design', *IEEE Antennas Propag. Mag.*, vol. 62, no. 4, pp. 82–93, Aug. 2020.

[12] W. M. Dorsey, A. I. Zaghloul, and M. G. Parent, 'Perturbed square-ring slot antenna with reconfigurable polarization', *IEEE Antennas Wirel. Propag. Lett.*, vol. 8, pp. 603–606, 2009.

[13] S.-G. Zhou, G.-L. Huang, H.-Y. Liu, A.-S. Lin, and C.-Y.-D. Sim, 'A CPW-fed square-ring slot antenna with reconfigurable polarization', *IEEE Access*, vol. 6, pp. 16474–16483, 2018.

[14] J. S. Herd and M. D. Conway, 'The evolution to modern phased array architectures', *Proc. IEEE*, vol. 104, no. 3, pp. 519–529, Mar. 2016.

[15] Z. Xiao *et al.*, 'Antenna array enabled space/air/ground communications and networking for 6G', *IEEE J. Sel. Areas Commun.*, vol. 40, no. 10, pp. 2773–2804, Oct. 2022.

[16] C. A. Balanis, *Antenna theory: analysis and design*, 3rd ed. Hoboken, NJ: John Wiley, 2005.

[17] R. L. Haupt, 'Thinned arrays using genetic algorithms', *IEEE Trans. Antennas Propag.*, vol. 42, no. 7, pp. 993–999, Jul. 1994.

[18] Y. Aslan, A. Roederer, and A. Yarovoy, 'System advantages of using large-scale aperiodic array topologies in future mm-Wave 5G/6G base stations: an interdisciplinary look', *IEEE Syst. J.*, pp. 1–10, 2021.

[19] D. Bianchi, S. Genovesi, and A. Monorchio, 'Constrained Pareto optimization of wide band and steerable concentric ring arrays', *IEEE Trans. Antennas Propag.*, vol. 60, no. 7, pp. 3195–3204, Jul. 2012.

[20] A. Kedar, 'Deterministic synthesis of wide scanning sparse concentric ring antenna arrays', *IEEE Trans. Antennas Propag.*, vol. 67, no. 12, pp. 7387–7395, Dec. 2019.

[21] Y.-Y. Bai, S. Xiao, M.-C. Tang, Z.-F. Ding, and B.-Z. Wang, 'Wide-angle scanning phased array with pattern reconfigurable elements', *IEEE Trans. Antennas Propag.*, vol. 59, no. 11, pp. 4071–4076, Nov. 2011.

[22] Y.-F. Cheng, X. Ding, W. Shao, M.-X. Yu, and B.-Z. Wang, 'A novel wide-angle scanning phased array based on dual-mode pattern-reconfigurable elements', *IEEE Antennas Wirel. Propag. Lett.*, vol. 16, pp. 396–399, 2017.

[23] D. Bianchi, S. Genovesi, and A. Monorchio, 'Randomly overlapped subarrays for reduced sidelobes in angle-limited scan arrays', *IEEE Antennas Wirel. Propag. Lett.*, vol. 16, pp. 1969–1972, 2017.

[24] M. Shadi, M. R. Tavakol, M. Alibakhshikenari, F. Arpanaei, and F. Falcone, 'Uniform overlap feeding network to reduce the number of phase shifters in scan arrays', in *2022 International Symposium on Antennas and Propagation (ISAP)*, Oct. 2022, pp. 541–542.

[25] B. Avser, J. Pierro, and G. M. Rebeiz, 'Random feeding networks for reducing the number of phase shifters in limited-scan arrays', *IEEE Trans. Antennas Propag.*, vol. 64, no. 11, pp. 4648–4658, Nov. 2016.

[26] P. Rocca, R. J. Mailloux, and G. Toso, 'GA-based optimization of irregular subarray layouts for wideband phased arrays design', *IEEE Antennas Wirel. Propag. Lett.*, vol. 14, pp. 131–134, 2015.

[27] L. W. Mou and Y. J. Cheng, 'Design of aperiodic subarrayed phased arrays with structural repetitiveness', *IEEE Trans. Antennas Propag.*, vol. 70, no. 12, pp. 11697–11706, Dec. 2022.

[28] X.-X. Li, W. Dong, Z.-H. Xu, and S.-P. Xiao, 'Hierarchical array design strategy composed of irregular and overlapped subarrays in large-scale planar array', *IEEE Trans. Antennas Propag.*, vol. 69, no. 7, pp. 4217–4222, Jul. 2021.

[29] N. Liu, S.-W. Qu, Y. Ma, and S. Yang, 'Irregular phased array architecture with small directivity drop for wide-angle scanning application', *IEEE Trans. Antennas Propag.*, vol. 70, no. 12, pp. 11617–11628, Dec. 2022.

[30] N. Anselmi, L. Tosi, P. Rocca, G. Toso, and A. Massa, 'A self-replicating single-shape tiling technique for the design of highly modular planar phased arrays—the case of L-shaped rep-tiles', *IEEE Trans. Antennas Propag.*, vol. 71, no. 4, pp. 3335–3348, Apr. 2023.

[31] Z.-Y. Xiong, Z.-H. Xu, S.-W. Chen, and S.-P. Xiao, 'Subarray partition in array antenna based on the algorithm x', *IEEE Antennas Wirel. Propag. Lett.*, vol. 12, pp. 906–909, 2013.

[32] H. Jiang, Y. Gong, J. Zhang, and S. Dun, 'Irregular modular subarrayed phased array tiling by algorithm X and differential evolution algorithm', *IEEE Antennas Wirel. Propag. Lett.*, pp. 1–5, 2023.

[33] F. A. Dicandia and S. Genovesi, 'Wide-scan and energy-saving phased arrays by exploiting penrose tiling subarrays', *IEEE Trans. Antennas Propag.*, vol. 70, no. 9, pp. 7524–7537, Sep. 2022.

[34] T. Isernia, M. D'Urso, and O. M. Bucci, 'A simple idea for an effective sub-arraying of large planar sources', *IEEE Antennas Wirel. Propag. Lett.*, vol. 8, pp. 169–172, 2009.

[35] R. Wang, B.-Z. Wang, C. Hu, and X. Ding, 'Wide-angle scanning planar array with quasi-hemispherical-pattern elements', *Sci. Rep.*, vol. 7, no. 1, p. 2729, Dec. 2017.

[36] A. Fenn, 'Theoretical and experimental study of monopole phased array antennas', *IEEE Trans. Antennas Propag.*, vol. 33, no. 10, pp. 1118–1126, Oct. 1985.

[37] F. A. Dicandia and S. Genovesi, 'Spectral efficiency improvement of 5G massive mimo systems for high-altitude platform stations by using triangular lattice arrays', *Sensors*, vol. 21, no. 9, p. 3202, May 2021.

[38] C. C. Coello, G. B. Lamont, and D. A. van Veldhuizen, *Evolutionary algorithms for solving multi-objective problems*. Springer Science & Business Media, 2007.

[39] A. Bagheri, C. Bencivenni, M. Gustafsson, and A. A. Glazunov, 'A 28 GHz 8 × 8 gapwaveguide phased array employing gan front-end with 60 dBm EIRP', *IEEE Trans. Antennas Propag.*, vol. 71, no. 5, pp. 4510–4515, May 2023.

[40] R. L. Haupt, *Antenna arrays: a computational approach*. Hoboken, N.J: Wiley-IEEE Press, 2010.

[41] N. Tervo *et al.*, 'Digital predistortion of phased-array transmitter with shared feedback and far-field calibration', *IEEE Trans. Microw. Theory Tech.*, vol. 69, no. 1, pp. 1000–1015, Jan. 2021.

[42] C. Fager, T. Eriksson, F. Barradas, K. Hausmair, T. Cunha, and J. C. Pedro, 'Linearity and efficiency in 5G transmitters: new techniques for analyzing efficiency, linearity, and linearization in a 5G active antenna transmitter context', *IEEE Microw. Mag.*, vol. 20, no. 5, pp. 35–49, May 2019.

[43] M. Y. Javed, N. Tervo, M. E. Leinonen, and A. Pärssinen, 'Wideband inter-beam interference cancellation for mmw/sub-thz phased arrays with squint', *IEEE Trans. Veh. Technol.*, pp. 1–13, 2023.

[44] M. Y. Javed, N. Tervo, M. E. Leinonen, and A. Pärssinen, 'Spatial interference reduction by subarray stacking in large two-dimensional antenna arrays', *IEEE Trans. Antennas Propag.*, pp. 1–1, 2020.

[45] W. P. M. N. Keizer, 'Fast low-sidelobe synthesis for large planar array antennas utilizing successive fast fourier transforms of the array factor', *IEEE Trans. Antennas Propag.*, vol. 55, no. 3, pp. 715–722, Mar. 2007.

[46] B. Rupakula, A. H. Aljuhani, and G. M. Rebeiz, 'Limited scan-angle phased arrays using randomly grouped subarrays and reduced number of phase shifters', *IEEE Trans. Antennas Propag.*, vol. 68, no. 1, pp. 70–80, Jan. 2020.

[47] S. A. Mitilineos, S. C. A. Thomopoulos, and C. N. Capsalis, 'On array failure mitigation with respect to probability of failure, using constant excitation coefficients and a genetic algorithm', *IEEE Antennas Wirel. Propag. Lett.*, vol. 5, pp. 187–190, 2006.